# Quantitative Super-Resolution Microscopy of Nanopipette-Deposited Fluorescent Patterns

**Simon Hennig,*,† Sebastian van de Linde,‡ Stephan Bergmann,† Thomas Huser,†,§ and Markus Sauer‡**

†Biomolecular Photonics, Department of Physics, University of Bielefeld, Universitätsstraße 25, 33615 Bielefeld, Germany, ‡Department of Biotechnology & Biophysics, Biozentrum, Julius Maximilians University Würzburg, Am Hubland, 97075 Würzburg, Germany, and §Department of Internal Medicine, NSF Center for Biophotonics, University of California, Davis, 2700 Stockton Boulevard, Suite 1400, Sacramento, California 95817, United States

**ABSTRACT** We describe a method for the deposition of minute amounts of fluorophore-labeled oligonucleotides with high local precision in conductive and transparent solid layers of poly(vinyl alcohol) (PVA) doped with glycerin and cysteamine (PVA-G-C layers). Deposition of negatively charged fluorescent molecules was accomplished with a setup based on a scanning ion conductance microscope (SICM) using nanopipettes with tip diameters of ~100 nm by using the ion flux flowing between two electrodes through the nanopipette. To investigate the precision of the local deposition process, we performed *in situ* super-resolution microscopy by *direct* stochastic optical reconstruction microscopy (*d*STORM). Exploiting the single-molecule sensitivity and reliability of *d*STORM, we determine the number of fluorescent molecules deposited in single spots. The correlation of applied charge and number of deposited molecules enables the quantification of delivered molecules by measuring the charge during the delivery process. We demonstrate the reproducible deposition of 3−168 fluorescent molecules in single spots and the creation of fluorescent structures. The fluorescent structures are highly stable and can be reused several times.

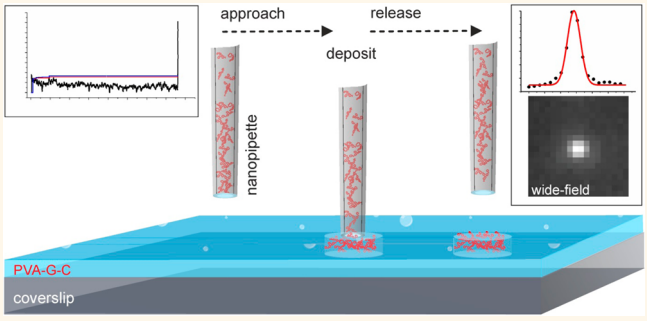


**KEYWORDS:** quantitative super-resolution microscopy · nanopipette · single-molecule deposition · scanning ion conductance microscopy (SICM) · *direct* stochastic optical reconstruction microscopy (*d*STORM)

The development of techniques that enable the precise deposition of biological molecules on the nanometer scale is of critical importance in the nanosciences.[1,2] Possible applications of such nanostructures or nanoassemblies range from highly parallelized bioassays,[3,4] the deposition of substrates for protein and nanoparticle crystallization,[5,6] to calibration samples for super-resolution fluorescence imaging,[7] and low-energy electron-induced bond dissociation.[8] Current methods for the production of small (bio)molecular structures include microcontact printing ($\mu$CP),[9] electron-beam lithography in combination with self-assembled monolayers,[10] and dip-pen nanolithography (DPN).[11,12] DPN uses scanning probe microscopy (SPM) techniques to create protein spots on surfaces by the tip of an atomic force microscope (AFM) acting as a nanosized fountain pen to transfer molecules from a reservoir onto the surface by capillary forces.

Nanostructures can also be produced in solution by ejecting negatively charged molecules *via* an electrochemical current onto a modified surface using scanning ion conductance microscopy (SICM).[13,14] In these experiments, spot sizes between 480 and 830 nm (fwhm) of fluorescently labeled and biotinylated DNA molecules deposited onto streptavidin-coated glass surfaces have been achieved. Alternatively, nanometer-sized patterns of proteins have been produced by deposition through cantilevered nanopipettes using SPM.[15] Inspection of the printed patterns by AFM shows that the method yields spot sizes of 200−500 nm in diameter.

In an attempt to produce even smaller fluorescent structures approaching molecular-scale resolution, DNA origami structures[7,16] and single-molecule cut-and-paste (SMCP)[17−19] methods have recently attracted considerable interest. Using SMCP, individual fluorescently labeled oligonucleotides can be arranged at

* Address correspondence to shennig@physik.uni-bielefeld.de.

Received for review April 14, 2015 and accepted July 14, 2015.

**Published online July 14, 2015**
**10.1021/acsnano.5b02220**

will on a surface by transferring them from a well to a target area by an AFM tip. As long as the number of deposited fluorescent molecules remains low (<10 molecules), their number and positions can be determined following individual photobleaching steps and fitting two-dimensional Gaussian functions to the reconstructed point-spread-function (PSF) of individual fluorophores.[19]

Here, we demonstrate the voltage-driven deposition of negatively charged, fluorescently labeled oligonucleotides into a modified solid and conductive PVA layer by utilizing a modified SICM with nanopipettes at a tip diameter of ~100 nm. To investigate the structure and to quantify the number of deposited molecules, we performed *direct* stochastic optical reconstruction microscopy (*d*STORM), a super-resolution imaging method with single molecule sensitivity employing standard fluorescent probes,[20−22] on these samples. The molecular deposition method operates in air and makes use of the ion current that flows, while the nanopipette is in contact with the surface of the modified PVA layer. The ion current between an electrode held within the pipet and a counter electrode embedded in the PVA layer serves as a feedback signal for tip−sample distance control and also controls the delivery of charged molecules to the surface. Once the contact with the surface is established, negatively charged oligonucleotides with the sequence (5′ → 3′): ATC GTT ACC AAA GCA TCG TAA ATC GCA TAA attached covalently to Alexa Fluor 647 (for further details see Supporting Information) are ejected into PVA by switching the potential between the electrodes. This creates nanometer-sized spots in the contact area. The method is fast compared to early nanopipette deposition techniques, which needed at least 10 s of deposition time for each spot[13] and single molecule cut and paste techniques, with a deposition time of at least 7 s for a single molecule.[18] In dip-pen nanolithography, the dwell time for deposition of molecules ranges from 0.5 to 60 s strongly affecting the deposition area from 0.1 to 0.8 $\mu m^2$.[23] Our deposition method enables the creation of fluorescent nanostructures on nonfunctionalized surfaces within 0.7−10 s depending on the spot size to be created (see also Supporting Information Figure S7b).

At the same time, the number of molecules deposited by this process can be precisely controlled by the concentration of charged fluorescent molecules inside the nanopipette, the electric potential, and the duration of the ejection process. We demonstrate the creation of different nanostructures consisting of single isolated fluorophore spots and quantify the number of deposited fluorophores per spot by *d*STORM. Furthermore, we show that the number of fluorescent molecules deposited within a single spot depends on the applied charge. The charge is calculated by multiplying the ion current with the contact time during deposition. We also demonstrate the possibility to reuse the layers for further investigation of the created structures.

## RESULTS

To "write" nanostructures, we utilize a modified SICM, a method which has originally been invented for topographic imaging of soft, nonconducting surfaces in aqueous solvents, *e.g.*, imaging of living cells.[24,25] SICM utilizes a $SiO_2$ nanopipette with small tip opening, which is filled with an electrolyte solution. The ionic current that begins to flow when a potential is applied between an electrode inside the pipet and a counter-electrode is used to create a height-dependent feedback signal to move the pipet stepwise over the surface while maintaining a constant distance.

In turn, and of significant interest for our current application, the nanopipette can also be used to directly deposit fluorophores conjugated to charged macromolecules onto a surface. On the basis of the voltage applied between tip and electrolyte bath, this permitted the precise deposition of an estimated number of 46,000 ± 12,000 molecules per spot onto a functionalized surface.[13] Due to the relatively large tip−surface distance of approximately 100 nm and due to the large diffusion lengths for molecules in electrolyte solutions, the spot size is typically limited to ~500 nm fwhm.[14] To minimize the lateral diffusion of molecules leaving the nanopipette and optimize the *d*STORM capability of the created nanostructures, we decided to perform the deposition in a layer of conducting polymer.

To accomplish this, we first create a mixture consisting of long-chain poly(vinyl alcohol) (PVA), glycerin, and cysteamine (PVA-G-C). Applying this solution to a glass substrate leads to a smooth, transparent and elastic layer on the glass surface with 1.0−1.5 $\mu$m thickness and a conductivity that can be measured with low noise laboratory current amplifiers. The elasticity of the surface also protects the tip from damage if the nanopipette contacts the surface.

The underlying principle of voltage-driven fluorophore deposition in a conductive polymer layer is schematically depicted in Figure 1. A nanopipette with a typical tip diameter of 100 nm is filled with 10 $\mu$L of a $10^{-7}$ M aqueous solution of oligonucleotides labeled with Alexa Fluor 647 and inserted into the pipet holder. The nanopipette is then manually positioned ~15 $\mu$m above the surface. Subsequently, a piezo-electric translation stage is used to approach the surface, while a potential of 0.2−1.0 V is applied to the electrode in the pipet and the counter electrode in the conductive polymer layer (Supporting Information Figure S1). As long as the nanopipette has not made contact with the surface, no ion current is detected. The nanopipette is then moved toward the surface in 1.5−3.0 nm steps while monitoring the ion current simultaneously.

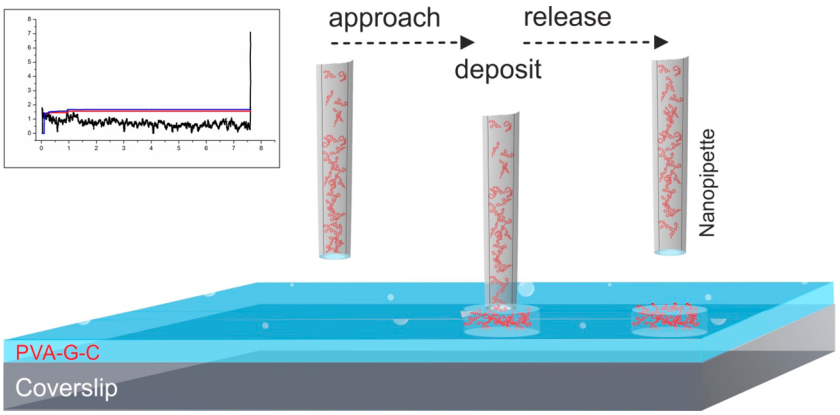


**Figure 1. Schematics of the molecular deposition process. A nanopipette filled with fluorescent oligonucleotides is placed manually several micrometers above the PVA-G-C surface. The microelectrodes are connected to the surface and the nanopipette (see Supporting Information Figure S1). A potential of several millivolts is applied to the electrodes, but no ion current is detected at this time. The ion current becomes detectable after the nanopipette approaches the surface (see inset). By reversing the potential or applying a higher voltage, the molecules are ejected out of the pipet into the surface. Following the localized delivery, the nanopipette is raised.**

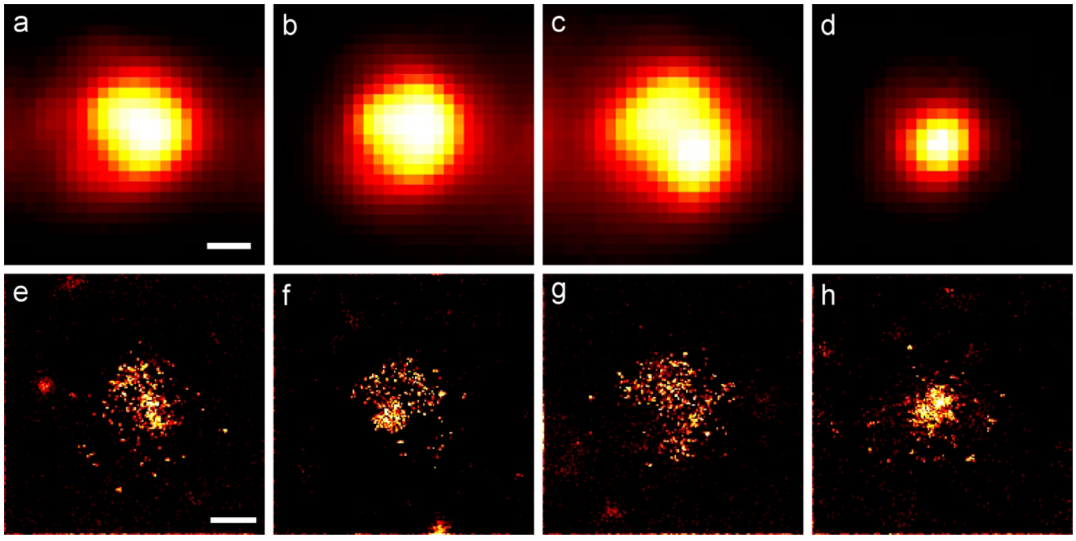


**Figure 2. Standard wide-field fluorescence (a–d) and corresponding *d*STORM images (e–h) of single fluorescent spots created with a potential of −50 mV and a contact time of 10 s at a concentration of $10^{-7}$ M Alexa Fluor 647 labeled oligonucleotides diluted in PBS in the nanopipette. Super-resolution images were reconstructed from 10,000 frames at an excitation power of 1 kW/cm$^2$ at 647 nm and an integration time of 40 ms per frame. *d*STORM reveals the distribution of fluorophores in each spot. Although every spot was deposited using the same conditions, it is readily apparent from the wide-field images that each spots has a different shape. The subsequently recorded *d*STORM images offer valuable clues about the detailed distribution of the molecules inside the deposited spots. (a–d) Average wide-field images of 50 single images taken at an excitation power of 350 W/cm$^2$ at 647 nm with an integration time of 100 ms. Scale bars, 300 nm.**

Upon contact with the surface, the ion current increases rapidly and the approach is stopped immediately (Supporting Information Figure S2).

To eject negatively charged fluorophore-labeled oligonucleotides, the software-controlled potential is switched to −10 to −500 mV leading to a negative ion current of typically −5 to −40 pA. After this reverse potential is applied for several seconds to deposit molecules, the pipet tip is retracted from the surface and returned to the original position for the next approach. For the "writing" of structures, the procedure is repeated several times. Due to the large amount of molecules inside the pipet, repeated delivery is possible.

The analysis of single fluorescent spots, deposited in rapid succession by using the same conditions, reveals a wide range of different spot sizes, shapes and distributions of molecules. Figure 2 shows four different representative spots, which were deposited under identical conditions (nanopipette, molecule concentration inside the pipet, approach and applied potential). The different size and shape of the spots are already visible in the wide-field fluorescence images. To evaluate the distribution of the molecules inside each single spot, we performed single-molecule localization microscopy by *d*STORM.[20] This is possible due to the presence of a millimolar concentration of

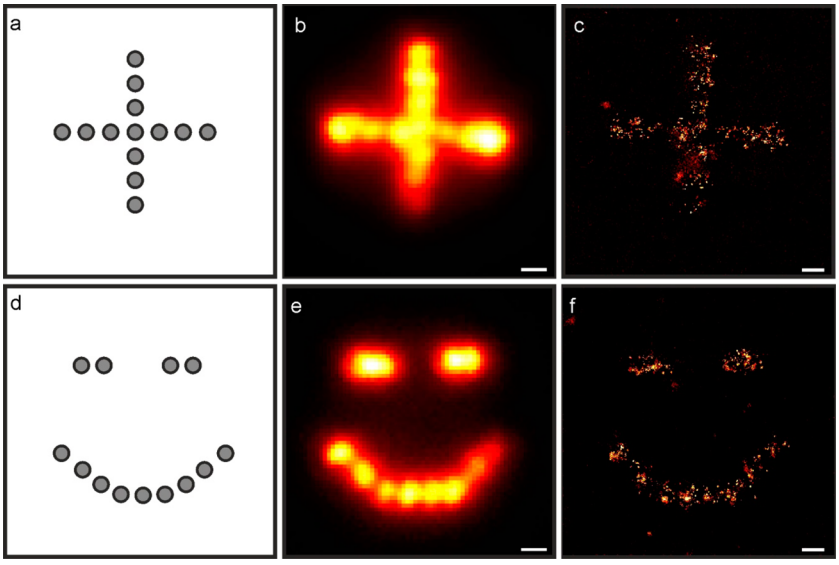


**Figure 3. Fluorophore spot pattern consisting of 13 individual spots arranged in a cross pattern and a smiley structure, respectively. (a and d) Cross and smiley structures are composed of a center-to-center-distance between the spots of 300 and 450 nm, respectively. The used concentration inside the nanopipette was $10^{-7}$ M of Alexa Fluor 647 labeled oligonucleotides diluted in PBS. The spots were deposited at an electric potential of −30 mV and a contact time of 3 s each. The ion current fluctuated from spot to spot between −5 and −30 pA. (b and e) Average wide-field fluorescence images of the structures (50 images taken at 350 W/cm$^2$, excitation at 647 nm). (c and f) Reconstructed *d*STORM images using 10,000 frames recorded at an excitation intensity of 1 kW/cm$^2$ with an integration time of 15 ms. Scale bars, (b and e) 600 nm, (c and f) 400 nm.**

cysteamine molecules in the polyvinyl layer. Besides influencing the conductive properties of the polymer layer, cysteamine creates a reductive environment, which is necessary to adjust the photoswitching rates of the deposited fluorophores for *d*STORM imaging. The resulting *d*STORM images clearly show the inhomogeneous distribution of delivered molecules. Among other causes, the inhomogeneity could be the result of an inhomogeneous local distribution of cysteamine in the PVA-G-C layer, which affects the direction of the ionic current.

To investigate the possibility to write fluorescent structures with high spatial resolution, we deposited fluorophores as individual spots forming a cross and a "smiley" structure with distances of 300 and 450 nm, respectively, in the PVA-G-C layer (Figures 3a,d). The individual spots were deposited with a potential of −30 mV and a contact time of 3 s. The ion current fluctuated from spot to spot between −5 and −30 pA. Individual spots of the cross deposited at a distance of 300 nm cannot be identified in the standard wide-field fluorescence image (Figure 3b). In contrast, some single spots in the smiley structure can be optically resolved because of their slightly larger spot distance of 450 nm (Figure 3e). The corresponding *d*STORM images (Figure 3c,f) of the two structures clearly show enhanced spatial resolution and reveal the local distribution of individual oligonucleotides within the polymer. To determine the lateral extent of the individual spots in the two structures, we histogrammed the full-width-at-half-maximum (fwhm) distribution for each spot from standard wide-field and *d*STORM images, respectively. For this, the position of every spot was taken from the blueprints (Figure 3a,d) and transferred to the wide-field and corresponding *d*STORM images.

Analysis of a total of 25 fluorescent deposited spots of the cross structure and the smiley structure revealed an average fwhm of 487 ± 51 nm (mean ± SD). For the total width of the deposited spot sizes in the corresponding *d*STORM images, we found a reduced spot diameter of 375 ± 70 nm (mean ± SD). These size measurements refer to the size of the actual deposited spot, not the fwhm of individual emitters. In case of the cross structure, the lowest lying spot could not be analyzed because of its low signal intensity, demonstrating that the deposition efficiency is strongly controlled by the nanoenvironment.

The number of localizations per spot retrieved from the *d*STORM images permits estimation of the numbers of molecules delivered per single spot. To translate the number of localizations into fluorophore numbers, the typical number of localizations detected per individual fluorophore under the applied experimental conditions has to be determined. Therefore, we prepared a calibration surface, consisting of the switching buffer containing a very low concentration of Alexa Fluor 647 labeled oligonucleotides (see Methods section). This leads to a surface with well isolated single fluorescent molecules on the surface. Using a standard imaging cycle of 10 000 single frames acquired with an integration time of 20 ms at 1 kW/cm$^2$, we then determined the number of localizations per isolated fluorescence signal.

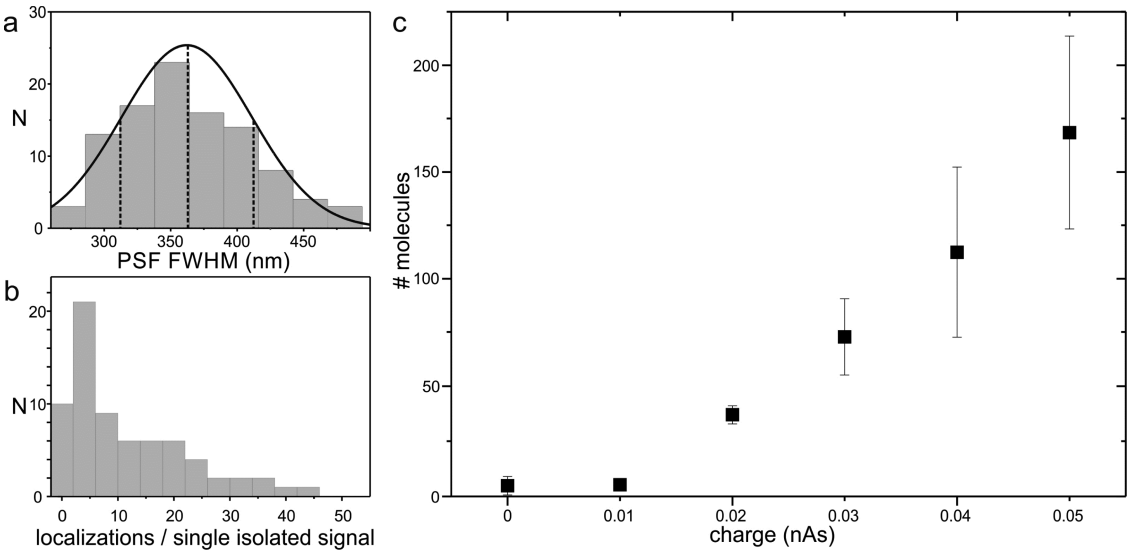


**Figure 4. (a) Frequency histogram of the fwhm of 101 isolated fluorescence signals within the calibration surface. Fitting to a Gaussian distribution, we defined a fluorescence signal as a single emitter, if the fwhm of the fluorescence signal lies within the standard deviation. The mean fwhm of the emitters was determined to be 362 nm. The standard deviation was located between 313 and 411 nm, respectively. (b) Frequency histogram of 88 selected molecules out of the PSF fitting process in (a). The mean localization number was determined to be 5.9 ± 0.5 for single emitters. (c) Quantitative delivery of Alexa Fluor 647 molecules to a PVA-G-C layer. Alexa 647 molecules were diluted in switching buffer inside the nanopipette. Single spots were created with a potential of −500 mV at different charge from 0.01 to 0.05 nAs. Single spots represent the mean value out of 6 measurements. The error bars represent the standard deviation of the mean values. The number of molecules delivered in a single spot ranges from 3.0 ± 1.5 to 168 ± 45 (see also Supporting Information Table S2).**

To determine the spatial resolution of the setup we first measured the fwhm of 100 nm Tetraspeck beads at an emission wavelength of 680 nm. This results in a fwhm of 360 nm. We then compared these data to the fwhm spot size obtained for isolated fluorescence signals on the calibration surface. We analyzed 101 isolated fluorescent signals of the calibration surface. The resulting frequency distribution shows a mean fwhm spot size of 362 ± 49 nm (mean ± SD) (Figure 4a), which is in good agreement with the value measured for single Tetraspeck beads. In the following, we defined all fluorescence signals with measured fwhm spot sizes in the range from 313 to 411 nm, (fwhm inside the standard deviation of the Gaussian fit of the frequency histogram), as isolated single fluorescent emitters and determined the localization statistics for these emitters using rapid*STORM.[26] Determining the number of localizations and generation of a frequency distribution of the resulting number (Figure 4b) leads to 5.9 ± 0.5 (mean ± SEM) localizations per fluorescence emitter in the calibration sample.

To estimate the number of molecules present per spot, we performed nanopipette-deposition experiments under identical conditions as used for the single-molecule calibration surface. Briefly, we changed the preparation procedure of the PVA stock solution resulting in increased cross-linking of the PVA strands during vaporization. Additionally, we reduced the glycerine ratio to improve the conductive properties of the surfaces and thus deliver more reliable results. Furthermore, we noticed that during the deposition process a local microenvironment underneath the tip is created, which mainly consists of the pipet-delivered buffer solution and molecules, which do not instantly interact with the surrounding PVA-G-C. To test this assumption, we deposited single spots with the nanopipette filled with either PBS or switching buffer. Both solutions contained a concentration of $10^{-7}$ M Alexa Fluor 647 labeled oligonucleotides. This implies that each spot should contain the same number of molecules.

The fluorescence signal created with PBS buffer shows a rapid signal decrease (Supporting Information Figure S3), whereas the spot created using switching buffer shows nearly constant fluorescence intensity for several minutes. In addition, *d*STORM experiments highlight the improved photoswitching behavior of Alexa Fluor 647 in the presence of switching buffer (Supporting Information Figure S4). These results suggest that the deposition of molecules is always accompanied by simultaneous delivery of the buffer solution. Overall, this strongly indicates the existence of a buffer microenvironment, which survives for at least 1 h.

The ionic current is always varying from spot to spot and fluctuating within every spot deposition (see Supporting Information Figure S6). This has to be taken into account when a fairly specific number of fluorophores shall be deposited at a given position simply by varying the delivery time at a constant voltage. To compensate for this, we measured the "charge", which sums up the ionic current for a defined period of time while the nanopipette is in contact with the surface.

**TABLE 1. Blinking Statistics of Single Alexa 647 Oligonucleotides Embedded in a PVA-G-C Surface[a]**

| day | 1 | 3 | 5 | 7 | 9 |
|---|---|---|---|---|---|
| no. localizations/isolated fluorescence signal (ident. Position) | 4 | 2.8 | 1.4 | 2.3 | 20 |
| no. localizations/isolated fluorescence signal (diff. position) | 4 | 1.6 | 1.7 | 3.0 | 5.9 |
| Signal to Noise Ratio | 4.3 ± 1.8 | 4.9 ± 2.3 | 5.8 ± 3 | 5.1 ± 2.9 | 5.0 ± 2.7 |

[a] The prepared surface was measured over 9 days, each with an excitation power of 1 kW/cm$^2$. In a selected area with multiple emitters 5000 frames were recorded on each measurement. The mean number of localizations for each isolated fluorescence signal inside the selected area was determined by employing the rapidSTORM software, summing up the total localizations, and dividing by the number of recognized single fluorescence signals. Two measurements were performed on the PVA-G-C surface. First, on identical areas (upper line) and, second, on different areas (lower line) for each measurement. Additionally, the signal to noise ratio of the fluorescent signals in the field of view was measured by determining the brightness against the global background for each isolated fluorescence signal. The average value of each measurement was plotted against the day subsequently. The errors represent the standard deviation.

To determine the number of molecules deposited in dependence of the predefined charge, we created a line of five spatially isolated fluorescent spots using a potential of −500 mV. To account for the spatially varying ionic current, we used a variable contact time for each spot at a predefined charge of 0.01, 0.02, 0.03, 0.04, and 0.05 nAs. Analysis of the wide-field fluorescence images indicates different fluorescence intensities and thus numbers of fluorophores present in each spot (Supporting Information Figure S5). To obtain sufficient statistics, we repeated the experiment six times and performed super-resolution imaging by *d*STORM at the standard imaging cycle (10,000 frames, 1 kW/cm$^2$, 20 ms) directly after the deposition. We find that we were able to deliver 3.0 ± 1.5 up to 168 ± 45 (mean ± SD) molecules per spot at a charge of 0.01−0.05 nAs using a concentration of $10^{-7}$ M Alexa Fluor 647 inside the nanopipette (Figure 4c and Supporting Information Table S2). These numbers are obtained by considering the mean localization frequency determined per single Alexa Fluor 647 molecule of 5.9 ± 0.5 (mean ± SEM). Our data show a linear increase of the number of delivered molecules with increasing charge (Figure 4c). Interestingly, on average 3 molecules are always delivered by the nanopipette to the layer upon contact even at zero charge (Figure 4c). In contrast, the wide-field fluorescence intensity plots saturate at higher charge (Supporting Information Figure S5). When analyzing the data, it has to be considered that the deposition area increases with increasing delivery time, which is not taken into account in the wide-field fluorescence intensity plots.

Our data clearly demonstrate that a modified SICM can be used successfully to write fluorescent structures composed of a few fluorophores confined to almost round spots with radii <200 nm. With the use of a smaller tip diameter and subsequent decreasing deposited spot size, the PVA-G-C surfaces have the capability to serve as reference samples for (super-resolution) fluorescence microscopy. Here, the stability of the fluorophore structure inside the PVA-G-C layer for repeated use and storage is of critical importance. To obtain data regarding the long-term stability of PVA-G-C structures, we mixed a $10^{-9}$ M aqueous solution of Alexa Fluor 647 with 10 μL of PVA-G-C solution and stored the sample at 4 °C. The photoswitching performance of spatially isolated single fluorescence signals was then investigated repeatedly during several days (Table 1).

Although the number of localizations per single fluorescence signal varies strongly from measurement to measurement, the fluorescence signals are not vanishing and the signal-to-noise ratio (SNR) remains constant in the different experiments within a range of 15% referred to the mean value. Besides the SNR, we also determined the number of localizations which fluctuated slightly from measurement to measurement with only one major deviation at day 9. Nevertheless, our findings demonstrate that fluorophore PVA-G-C structures prepared by delivery of fluorophore labeled oligonucleotides from nanopipettes could be stored for several days without apparent loss in photoswitching performance. Since the photoswitching mechanism of most fluorophores is based on collisional quenching of the fluorophore's triplet state by thiolate and the formation of stable semireduced or fully reduced leuco fluorophores,[27] our data indicate that the polymer-embedded aqueous samples do not dry out during 9 days of storage at 4 °C.

## CONCLUSIONS AND OUTLOOK

We introduced a new and reliable method for accurate deposition of small numbers of fluorescent molecules in spatially confined spots to a solid surface, which enables reversible photoswitching of organic dyes. Analysis of the created spot widths reveals a fwhm of 487 nm using conventional wide-field imaging. This confirms the findings of Rodolfa *et al.*[14] with a minimal spot size of 480 nm fwhm, that deposition with nanopipettes operating in air on dry surfaces leads to a considerably smaller spot size compared to liquid based deposition, where the spot size is limited to 830 nm fwhm.[13] Further analysis of the super-resolved images reveals a fwhm of 375 nm and we were able to investigate the distribution of fluorescent molecules in nanopipette-deposited spots. In combination with reference experiments, the *d*STORM imaging allowed us to count the number of deposited fluorescent molecules. Since the number of delivered

molecules depends linearly on the applied charge, 3−168 fluorescently labeled oligonucleotides can be reproducibly deposited per spot simply by predefining the applied charge. Here, in contrast to previous experiments which were able to do a rough estimation of delivered molecules by counting the flow of fluorescent molecules through a focal volume and simultaneous counting the fluorescence events or intensity, we were able to make a more precise prediction of the delivered fluorescent molecules by single molecule localization microscopy including a previously performed calibration step. This makes nanopipette-assisted delivery on PVA-G-C surfaces a useful tool also for nanopipette-based delivery methods like nanoinjection[28,29] or other local delivery methods.[30] It is possible to predefine and estimate the overall number of molecules delivered onto or into biological targets with high precision by counting the delivered charge. To accomplish this, calibration measurements with the molecules to be delivered have to be performed beforehand at the desired concentration. Additionally, the range of delivered molecules can be influenced by adjusting the concentration of molecules inside the nanopipette. Furthermore, due to the solid structure of PVA-G-C surfaces, they can be easily handled and stored without any apparent loss in photoswitching performance over several days. Compared to other deposition techniques, nanopipette-based deposition can be realized fairly easily on any fluorescence microscope. On the basis of the fact that quantification of protein copies in cells becomes increasingly important,[31−36] nanopipette-deposited patterns can be used advantageously as calibration structures for quantitative super-resolution microscopy.

## METHODS

**Dyes.** Ten bases oligo single-stranded DNA labeled with Alexa Fluor 647 was purchased from IBA GmbH (Göttingen Germany). Purification grade: "Reverse Phase", 0.2 $\mu$M stock solution. Sequence (5′ → 3′): ATC GTT ACC AAA GCA TCG TAA ATC GCA TAA.

**Preparation of Nanopipettes.** Nanopipette tips with an average inner tip diameter of ∼100 nm were made from borosilicate glass capillaries with an outer diameter of 1.00 mm and an inner diameter of 0.58 mm (GB100F-10; Science Products, Germany). The pipet tips were pulled with a pipet puller P-2000 (Sutter Instrument; Novato, CA) and backfilled with 10 $\mu$L of Alexa Fluor 647 labeled DNA at a concentration of $10^{-6}$ M dissolved in pure $H_2O$. For quantitative *d*STORM experiments, 10 $\mu$L of $10^{-7}$ M Alexa647 oligo solved in the PCD switching buffer at a concentration described in Supporting Information Table S3 was backfilled into the nanopipette. Measurements of the inner tip diameter of ∼100 nm and the pulling procedure can be found in Bruckbauer *et al.*[13]

**Preparation of Ag-Electrodes.** Silver wire for the electrodes was purchased from Science Products, Gemany (AG-8T), cut in pieces of 3 cm in length and incubated in NaOCl for 30 min. Then, the silver wire pieces were carefully inserted and fixed in the preamplifier stage of the microelectrode amplifier.

**Setup.** The voltage driven deposition of dyes was made by a custom build setup, containing a patch clamp amplifier Axopatch 200B (Axon instruments; Sunnyvale, CA) and a 3D-piezo stage (Mad City Laboratories; Madison, WI) controlled by a home build Labview software (LabView V8.2, National Instruments).

Wide-field images were acquired by a 60× 1.49NA TIRF-objective (Olympus) mounted on an Olympus IX71 inverted microscope equipped with an electron multiplying CCD camera (ixon+ DU-888E, Andor Technology; Belfast, Northern Ireland). Dyes were excited by an ArKr+-Laser operating at 647 nm (Coherent innova 70C spectrum). Fluorescence light was separated by a beam splitter (560/659; Semrock; Rochester, NY) and a 647 long pass filter (RazorEdge, 647RU; Semrock) in the detection pathway. *d*STORM images were reconstructed with rapidSTORM (v2.20).[26]

**Preparation of PVA-G-C Surfaces.** Poly(vinyl alcohol) (PVA) was purchased from Sigma-Aldrich (341584). A volume of 100 $\mu$L of a saturated PVA-H2O solution was mixed with 100 $\mu$L of $H_2O$, then 1 $\mu$L of glycerin and subsequently 16 $\mu$L of cysteamine (1 M solution in $H_2O$) (30070, Sigma-Aldrich) were added.

Commercially available coverslips (∼150 $\mu$m), 24 × 60 $mm^2$ in size were carefully cleaned with HelmanexIII (Hellma GmbH, Germany) for 20 min in a supersonic bath at 45 °C. Then, the coverslips were rinsed for 2 times with pure $H_2O$, followed by another 20 min in a supersonic bath in pure $H_2O$. Then, the coverslips were dried in an air flow before use. A silicone sheet (self-adhesive) (Sigma-Aldrich (GBL666182-5EA)) with a hole of 4 mm in diameter was disposed to the coverslip. Ten microliters of the previously mixed solution was brought on the coverslip and dried headfirst overnight at 4 °C. Thereby, not every prepared surface shows adequate conducting properties. The measured ion current of single surfaces ranges from 2 to 200 pA at a potential of 1 V applied to the electrodes.

**Preparation of Surfaces for Quantitative Super-Resolution Experimtents.** *Preparation of PVA Stock solution.* For preparation of the stock solution for PVA-G-C surfaces, 4 g of poly(vinyl alcohol) (PVA) powder with a molecular weight of 72,000 g/M was stirred in 96 mL of double-distilled water at room temperature. Then, the temperature was increased to 80 °C. Dissolved and clump-free PVA was cooled to approximately 35 °C before decanting it into a 50 mL tube. This PVA solution is referred to as PVA 4%.

*Preparation of PVA-G-C Surfaces.* The following were combined: 400 $\mu$L of $H_2O$, 400 $\mu$L of 4% PVA, 1 $\mu$L of glycerol, and 160 $\mu$L of 1 M cysteamine. The final solution was mixed with a vortex mixer. Ten microliters was placed on a coverglass. To obtain a transparent and soft surface, the sample was dried for 2−3 days at 4 °C. Afterward, only a small amount of water remained in the sample due to the presence of glycerol. The formerly round drops on the coverglass changed to flat spots with a thickness between 1.0 and 1.5 $\mu$m. Freshly prepared samples can be used for maximum 2 weeks if stored at 4 °C.

*Preparation of PCD Stock Solution.* For the localization experiments, we used a switching buffer based on the enzymatic reaction between protocatechuate 3,4-dioxygenase (PCD) and 3,4-dihydroxybenzoic acid. The buffer was chosen instead of the commonly used glucose oxidase/catalase system due to its pH stability.[37] We increased the pH by using 500 mM Tris-HCl to 8.66.

For the end volume of 1.5 mL of PCD stock solution with an enzyme concentration of 1 mg/mL, the following components listed in Supporting Information Table S3 with the stated quantities were used. In the first step, 1.5 mg of PCD was dissolved in 372 $\mu$L of 50 mM Tris-acetate buffer which is adjusted to pH 7.5, and afterward, the substances with the given quantities from Supporting Information Table S3 were added. The resulting 1.5 mL PCD stock solution was divided into 15 aliquots of 100 $\mu$L and stored at −20 °C. To complete the components for the oxygen scavenger system, the 3,4-dihydroxybenzoic acid was dissolved in twice distilled water to a concentration of 125 mM.

*Preparation of Final Switching Buffer.* For the final switching buffer, 15 $\mu$L of 1 M 2-mercaptoethanol, 125 mM 3,4-dihydroxybenzoic acid, 25 $\mu$L of PCD stock solution, and 66 $\mu$L of 50 mM

Tris-acetate buffer at pH 7.5 were mixed. For use in nanopipettes, typically 30 $\mu$L was used. The given mixture has an end volume of 150 $\mu$L and can be adjusted to the desired amount and the final dye concentration for different applications like a single molecule surface or deposit fluorophores on a surface.

*Preparation of Calibration Samples.* For single molecule surfaces, a Lab-Tek was cleaned with 5% (v/v) Hellmanex III in twice distilled water for at least 30 min at 40 °C in an ultrasonic bath. Afterward, the cleaned chambers were washed three times with PBS. One spattle (~0.5 mg) Bovine Serum Albumin (BSA) (A2153, Sigma-Aldrich) and 1/3 spattle (~0.2 mg) biotin labeled BSA (A8549, Sigma-Aldrich) were dissolved in 2 mL of twice distilled water at 4 °C. Then, 500 $\mu$L of the solution was filled into the chambers. Then, the solution was incubated for at least 4 h in the fridge at 4 °C, or overnight. In the next step, 1/3 spattle Streptavidin (S4762, Sigma-Aldrich) was dissolved in 2 mL of twice distilled water at 4 °C. The previously applied BSA/BSA-biotin solution was carefully removed and refilled with the streptavidin solution. The surface should not dry out. Next, the LabTek was placed in the fridge at 4 °C for incubation for at least 4 h or overnight. After 3 washing steps with PBS, 200 $\mu$L of switching buffer with Alexa Fluor 647 coupled DNA (10 base pair, single-stranded, biotinylated) in a final concentration of $10^{-10}$ M was added to the well. The surfaces without added switching buffer and dye can be stored at 4 °C and used several times.

*Conflict of Interest:* The authors declare no competing financial interest.

*Supporting Information Available:* Electrode setup for the deposition experiments; typical approach curve for nanopipette-based delivery of molecules to a PVA-G-C layer; comparison between the fluorescence intensity of two spots created with switching buffer and PBS as solvent inside the nanopipette; wide-field images and intensity plots of nanopipette deposited spots of Alexa Fluor 647 oligonucleotides and list of fwhm values of such spots; list of localization statistics of single molecules deposited in spots; tracking of ion current during delivery of single spots created with Alexa Fluor 647 oligonucleotides; correlation between applied potential and average ion current, and applied potential and the average delivery time; localization statistics of single molecules deposited in spots. The Supporting Information is available free of charge on the ACS Publications website at DOI: 10.1021/acsnano.5b02220.

## REFERENCES AND NOTES


1. Whitesides, G. M.; Ostuni, E.; Takayama, S.; Jiang, X.; Ingber, D. E. Soft Lithography in Biology and Biochemistry. *Annu. Rev. Biomed. Eng.* **2001**, *3*, 335–373.
2. Willner, I. I.; Katz, E. Integration of Layered Redox Proteins and Conductive Supports for Bioelectronic Applications. *Angew. Chem., Int. Ed.* **2000**, *39*, 1180–1218.
3. Lockhart, D. J.; Winzeler, E. A. Genomics, Gene Expression and DNA Arrays. *Nature* **2000**, *405*, 827–836.
4. MacBeath, G.; Schreiber, S. L. Printing Proteins as Microarrays for High-Throughput Function Determination. *Science* **2000**, *289*, 1760–1763.
5. Nykypanchuk, D.; Maye, M. M.; van der Lelie, D.; Gang, O. DNA-Guided Crystallization of Colloidal Nanoparticles. *Nature* **2008**, *451*, 549–552.
6. Park, S. Y.; Lytton-Jean, A. K.; Lee, B.; Weigand, S.; Schatz, G. C.; Mirkin, C. A. DNA-Programmable Nanoparticle Crystallization. *Nature* **2008**, *451*, 553–556.
7. Steinhauer, C.; Jungmann, R.; Sobey, T. L.; Simmel, F. C.; Tinnefeld, P. DNA Origami as a Nanoscopic Ruler for Super-Resolution Microscopy. *Angew. Chem., Int. Ed.* **2009**, *48*, 8870–8873.
8. Keller, A.; Bald, I.; Rotaru, A.; Cauet, E.; Gothelf, K. V.; Besenbacher, F. Probing Electron-Induced Bond Cleavage at the Single-Molecule Level Using DNA Origami Templates. *ACS Nano* **2012**, *6*, 4392–4399.
9. James, C. D.; Davis, R. C.; Kam, L.; Craighead, H. G.; Isaacson, M.; Turner, J. N.; Shain, W. Patterned Protein Layers on Solid Substrates by Thin Stamp Microcontact Printing. *Langmuir* **1998**, *14*, 741–744.
10. Biebricher, A.; Paul, A.; Tinnefeld, P.; Golzhauser, A.; Sauer, M. Controlled Three-Dimensional Immobilization of Biomolecules on Chemically Patterned Surfaces. *J. Biotechnol.* **2004**, *112*, 97–107.
11. Lee, K. B.; Lim, J. H.; Mirkin, C. A. Protein Nanostructures Formed Via Direct-Write Dip-Pen Nanolithography. *J. Am. Chem. Soc.* **2003**, *125*, 5588–5589.
12. Piner, R. D.; Zhu, J.; Xu, F.; Hong, S.; Mirkin, C. A. "Dip-Pen" Nanolithography. *Science* **1999**, *283*, 661–663.
13. Bruckbauer, A.; Ying, L.; Rothery, A. M.; Zhou, D.; Shevchuk, A. I.; Abell, C.; Korchev, Y. E.; Klenerman, D. Writing with DNA and Protein Using a Nanopipet for Controlled Delivery. *J. Am. Chem. Soc.* **2002**, *124*, 8810–8811.
14. Rodolfa, K. T.; Bruckbauer, A.; Zhou, D.; Korchev, Y. E.; Klenerman, D. Two-Component Graded Deposition of Biomolecules with a Double-Barreled Nanopipette. *Angew. Chem., Int. Ed.* **2005**, *44*, 6854–6859.
15. Taha, H.; Marks, R. S.; Gheber, L. A.; Rousso, I.; Newman, J.; Sukenik, C.; Lewis, A. Protein Printing with an Atomic Force Sensing Nanofountainpen. *Appl. Phys. Lett.* **2003**, *83*, 1041–1043.
16. Rothemund, P. W. Folding DNA to Create Nanoscale Shapes and Patterns. *Nature* **2006**, *440*, 297–302.
17. Cordes, T.; Strackharn, M.; Stahl, S. W.; Summerer, W.; Steinhauer, C.; Forthmann, C.; Puchner, E. M.; Vogelsang, J.; Gaub, H. E.; Tinnefeld, P. Resolving Single-Molecule Assembled Patterns with Superresolution Blink-Microscopy. *Nano Lett.* **2010**, *10*, 645–651.
18. Kufer, S. K.; Puchner, E. M.; Gumpp, H.; Liedl, T.; Gaub, H. E. Single-Molecule Cut-and-Paste Surface Assembly. *Science* **2008**, *319*, 594–596.
19. Kufer, S. K.; Strackharn, M.; Stahl, S. W.; Gumpp, H.; Puchner, E. M.; Gaub, H. E. Optically Monitoring the Mechanical Assembly of Single Molecules. *Nat. Nanotechnol.* **2009**, *4*, 45–49.
20. Heilemann, M.; van de Linde, S.; Schuttpelz, M.; Kasper, R.; Seefeldt, B.; Mukherjee, A.; Tinnefeld, P.; Sauer, M. Subdiffraction-Resolution Fluorescence Imaging with Conventional Fluorescent Probes. *Angew. Chem., Int. Ed.* **2008**, *47*, 6172–6176.
21. van de Linde, S.; Heilemann, M.; Sauer, M. Live-Cell Super-Resolution Imaging with Synthetic Fluorophores. *Annu. Rev. Phys. Chem.* **2012**, *63*, 519–540.
22. van de Linde, S.; Loschberger, A.; Klein, T.; Heidbreder, M.; Wolter, S.; Heilemann, M.; Sauer, M. Direct Stochastic Optical Reconstruction Microscopy with Standard Fluorescent Probes. *Nat. Protoc.* **2011**, *6*, 991–1009.
23. Weeks, B. L.; Noy, A.; Miller, A. E.; De Yoreo, J. J. Effect of Dissolution Kinetics on Feature Size in Dip-Pen Nanolithography. *Phys. Rev. Lett.* **2002**, *88*, 255505.
24. Hansma, P. K.; Drake, B.; Marti, O.; Gould, S. A.; Prater, C. B. The Scanning Ion-Conductance Microscope. *Science* **1989**, *243*, 641–643.
25. Klenerman, D.; Korchev, Y. E.; Davis, S. J. Imaging and Characterisation of the Surface of Live Cells. *Curr. Opin. Chem. Biol.* **2011**, *15*, 696–703.
26. Wolter, S.; Loschberger, A.; Holm, T.; Aufmkolk, S.; Dabauvalle, M. C.; van de Linde, S.; Sauer, M. Rapidstorm: Accurate, Fast Open-Source Software for Localization Microscopy. *Nat. Methods* **2012**, *9*, 1040–1041.
27. van de Linde, S.; Krstic, I.; Prisner, T.; Doose, S.; Heilemann, M.; Sauer, M. Photoinduced Formation of Reversible Dye Radicals and Their Impact on Super-Resolution Imaging. *Photochem. Photobiol. Sci.* **2011**, *10*, 499–506.
28. Adam Seger, R.; Actis, P.; Penfold, C.; Maalouf, M.; Vilozny, B.; Pourmand, N. Voltage Controlled Nano-Injection System for Single-Cell Surgery. *Nanoscale* **2012**, *4*, 5843–5846.
29. Hennig, S.; van de Linde, S.; Lummer, M.; Simonis, M.; Huser, T.; Sauer, M. Instant Live-Cell Super-Resolution Imaging of Cellular Structures by Nanoinjection of Fluorescent Probes. *Nano Lett.* **2015**, *15*, 1374–1381.
30. Bruckbauer, A.; James, P.; Zhou, D.; Yoon, J. W.; Excell, D.; Korchev, Y.; Jones, R.; Klenerman, D. Nanopipette Delivery of Individual Molecules to Cellular Compartments for

Single-Molecule Fluorescence Tracking. *Biophys. J.* **2007**, *93*, 3120–3131.
31. Buxbaum, A. R.; Wu, B.; Singer, R. H. Single Beta-Actin Mrna Detection in Neurons Reveals a Mechanism for Regulating Its Translatability. *Science* **2014**, *343*, 419–422.
32. Cai, L.; Friedman, N.; Xie, X. S. Stochastic Protein Expression in Individual Cells at the Single Molecule Level. *Nature* **2006**, *440*, 358–362.
33. Ehmann, N.; van de Linde, S.; Alon, A.; Ljaschenko, D.; Keung, X. Z.; Holm, T.; Rings, A.; DiAntonio, A.; Hallermann, S.; Ashery, U.; Heckmann, M.; Sauer, M.; Kittel, R. J. Quantitative Super-Resolution Imaging of Bruchpilot Distinguishes Active Zone States. *Nat. Commun.* **2014**, *5*, 4650.
34. Fricke, F.; Malkusch, S.; Wangorsch, G.; Greiner, J. F.; Kaltschmidt, B.; Kaltschmidt, C.; Widera, D.; Dandekar, T.; Heilemann, M. Quantitative Single-Molecule Localization Microscopy Combined with Rule-Based Modeling Reveals Ligand-Induced Tnf-R1 Reorganization toward Higher-Order Oligomers. *Histochem. Cell Biol.* **2014**, *142*, 91–101.
35. Loschberger, A.; Franke, C.; Krohne, G.; van de Linde, S.; Sauer, M. Correlative Super-Resolution Fluorescence and Electron Microscopy of the Nuclear Pore Complex with Molecular Resolution. *J. Cell Sci.* **2014**, *127*, 4351–4355.
36. Yu, J.; Xiao, J.; Ren, X.; Lao, K.; Xie, X. S. Probing Gene Expression in Live Cells, One Protein Molecule at a Time. *Science* **2006**, *311*, 1600–1603.
37. Aitken, C. E.; Marshall, R. A.; Puglisi, J. D. An Oxygen Scavenging System for Improvement of Dye Stability in Single-Molecule Fluorescence Experiments. *Biophys. J.* **2008**, *94*, 1826–1835.